Thermal radiation and fragmentation pathways of photo-excited silicon clusters

Piero Ferrari, Ewald Janssens, Peter Lievens, and Klavs Hansen

Citation: The Journal of Chemical Physics **143**, 224313 (2015); doi: 10.1063/1.4936917
View online: http://dx.doi.org/10.1063/1.4936917
View Table of Contents: http://scitation.aip.org/content/aip/journal/jcp/143/22?ver=pdfcov
Published by the AIP Publishing

Thermal radiation and fragmentation pathways of photo-excited silicon clusters

Piero Ferrari,[1] Ewald Janssens,[1] Peter Lievens,[1] and Klavs Hansen[2]
[1]*Laboratory of Solid State Physics and Magnetism, KU Leuven, 3001 Leuven, Belgium*
[2]*Department of Physics, University of Gothenburg, 41296 Gothenburg, Sweden and Department of Physics and Astronomy, Aarhus University, 8000 Aarhus C, Denmark*

(Received 6 August 2015; accepted 19 November 2015; published online 9 December 2015)

The fragmentation of laser heated silicon clusters was studied by time-of-flight mass spectrometry. For Si_n^+ (n = 5–19, 21), the lowest energy fragmentation pathways were identified as the metastable decay channel occurring after the primary acceleration of the ions. The radiative cooling of laser excited Si_n^+ (n = 5–9, 11, and 13) was quantified via its quenching effect on the amount of metastable fragmentation. The quenching varied strongly with cluster size, from no observable amount for Si_7^+ to a cooling constant of $3 \cdot 10^5$ s^{-1} for Si_{13}^+. In addition, based on the observed fragmentation channels, the ionization energies and the relative binding energies of the clusters were partially ordered, and several ionization energies have been bracketed more precisely. © *2015 AIP Publishing LLC.* [http://dx.doi.org/10.1063/1.4936917]

INTRODUCTION

For strongly bound nanoparticles and clusters, thermal radiation can have a very strong stabilizing effect on highly excited particles, and is potentially an important factor in determining their abundances in non-equilibrium production processes involving such high excitation energies. Microsecond timescale radiative cooling has been observed from clusters of refractory metals[1–3] and fullerenes.[4] Radiation has even been measured in a number of fullerene anions, with their relatively loosely bound excess electron, albeit on a much longer timescale (several milliseconds).[5,6] The activation energy of the lowest energy decay channels, that indirectly sets the upper limit of the temperature of the particles, ranges between 2.7 eV for the electron affinity of C_{60}, to above 10 eV for C_2 loss from the neutral C_{60}.

Thermal radiation will tend to enhance the abundances of the strongly radiating particle sizes at the expense of less radiative sizes. It will therefore also seriously influence the conclusions with respect to the stability of clusters one draws from observations of "magic numbers" in mass spectra. In spite of the number of materials that are known to radiate thermally, the quantitative determination of radiative parameters for size selected clusters has received little attention, with the notable exception of carbon[5,6] and more recently niobium.[3] The question is of particular relevance for the production of technologically interesting size-selected clusters, because these tend to be composed of refractory materials. Silicon clusters have relatively high binding energies,[7] around 4 eV, albeit reduced in a region around n = 20, suggesting that radiative cooling may be important for at least some of these particles too. In addition, a correct assignment of the thermal radiation and lowest energy fragmentation channels as a function of cluster size will provide benchmark data for theoretical methods, with repercussions for calculations also for larger systems.

Historically, silicon clusters have been studied extensively, partly because of the material's technological applications.[7–38] The study of small silicon clusters was only made possible by the introduction of laser ablation cluster sources. From the first observations of silicon clusters in molecular beams,[8,9] their special fragmentation behavior attracted attention.[10–12] It was shown, for instance, that Si_6^+ is a favored photo-fragmentation product of small Si_n^+ ($n \leq 12$) clusters,[11] that Si_n^+ (n = 12–30) clusters give daughter ions of about one half to two thirds of the original size, and that larger clusters suffer extensive fragmentation to yield charged fragments composed of 6–11 atoms.[18] Bulk silicon, in contrast, evaporates monomers: 90% of silicon gas is atomic.[13]

The nature of the fragmentation pattern of silicon clusters was surmised to be largely independent of the excitation mechanism, because similar, albeit not identical, results were obtained by photo-excitation using different laser wavelengths[11,18] and by collision induced dissociation (CID).[7,20] Experimental dissociation energies could be inferred from disappearance energies in CID experiments,[7] demonstrating the enhanced stability of Si_6^+ and Si_{10}^+, and that the fragmentation channels of Si_n^+ (n = 12–25) are correlated with relative stabilities of fragments composed of 6–11 atoms. A study of soft X-ray photo-excitation of Si_n^+ (n = 9–19, 22–27)[39] showed multiple charge states, but it was also observed that the process produced Si_6^+, Si_7^+, Si_{10}^+, and Si_{11}^+ fragments for larger clusters.

Computational studies have addressed the fragmentation pathways and dissociation energies,[25,31,35] indicating a preference of silicon clusters composed of more than eight atoms to disintegrate by losing relatively large fragments, reproducing the general features of the experimental findings as they were known at the time.

Efforts have also been made to correlate the size-dependent stability to the geometrical structures of the clusters. Small silicon clusters (n = 4, 6, 7) deposited in an inert matrix were

studied by Raman spectroscopy.[23] Ion mobility measurements have provided information on the shapes of charged silicon clusters.[26,29] More recently, infrared multiple photon dissociation experiments have provided conclusive structural assignments of the neutral (n = 6–10, 15) and cationic (n = 6–11, 13-18) clusters.[36,38] The same technique has also been used to study the influence of a single dopant atom on the structure of the clusters.[40–44] Density functional theory (DFT) calculations have been used to explore the lowest energy configurations of silicon clusters in different charge states.[28,30–34] Second energy differences, as a measure of the relative stability of clusters, were calculated and provided local maxima for neutral Si_n (n = 6, 7, 10)[30] and cationic Si_n^+ (n = 6, 7, 11),[31] in agreement with the experimental findings. However, an intuitive correlation between stability and structure of silicon clusters is not yet available.

In summary, the present study was motivated by the dual purpose of finding the lowest energy fragmentation channels and measuring the radiative cooling of small, cationic silicon clusters, providing essential information for understanding of their size-dependent properties.

EXPERIMENTAL PROCEDURE

The procedure used here was, in brief, to multi-photon ionize and excite neutral clusters, extract the ions with an electric field which is switched on with or without a time delay after the laser pulse, and measure the metastable (i.e., delayed) fragmentation of the ions in the field-free region after acceleration.

The clusters were produced in a laser vaporization source,[45] operated with a pulsed Nd:YAG laser (532 nm, 10 Hz) providing pulse energies of 15-25 mJ. Helium gas at a backing pressure of 7 bars was introduced by a pulsed supersonic valve into a waiting room just before laser ablation of a silicon target, which was a piece of a commercial, high purity wafer. The clusters were thermalized by the helium to room temperature. This left the clusters with an internal energy much below the threshold for unimolecular dissociation on the relevant experimental timescales. After adiabatic expansion and passage through a conical skimmer, the beam entered the extraction region of a reflectron time-of-flight (TOF) mass spectrometer. The apparatus is schematically presented in Fig. 1. The charged clusters produced in the source were prevented from entering the extraction region by raising the first extractor grid downstream from the source to a positive potential of 10 V, except when the cation distribution from the source was probed. The remaining (neutral) clusters were ionized and photo-fragmented by an intense pulse of UV light (3rd harmonic of a Nd:YAG laser, 355 nm, 10 Hz). The laser beam had a diameter of 6 ± 1 mm and excited and ionized the clusters in the first field of the two-field ion extraction. The laser pulse energy, measured with a pyroelectric energy sensor, corresponded to a fluence above 100 mJ/cm^2. The fragmentation of the photo-excited clusters was extensive. Measuring the size distribution of cationic clusters produced in the source, i.e., without the 10 V blocking potential, showed no clusters below $n \approx 20$. With the 10 V blocking potential and after the combined multi-photon ionization and heating by the laser, the distribution peaked between n = 6 and n = 11. Mass spectra of the clusters were typically averaged over 10^4 laser pulses.

After acceleration and free flight at ground potential, the clusters entered the reflectron. The reflectron consists of two fields of different strength, a short and strong entry field, and a longer and weaker field where the clusters spent most of their time inside the reflectron. After exiting the reflectron, the clusters again moved through the field-free region and finally hit the primary detector. The delayed (metastable) fragmentation measured was the statistical decay that occurred after the initial acceleration in the TOF mass spectrometer and before entry into the reflectron.

In order to identify the parent and the charged daughter product of the metastable decay, the two potentials of the reflectron electrodes were varied proportionally. This is parametrized by the single parameter α, where the value α = 1 corresponds to the optimal mass resolution of the mass spectrometer. This situation is presented in panel (a) of Fig. 2, in which both promptly produced cluster size n and the metastable fragmentation product with the same size are

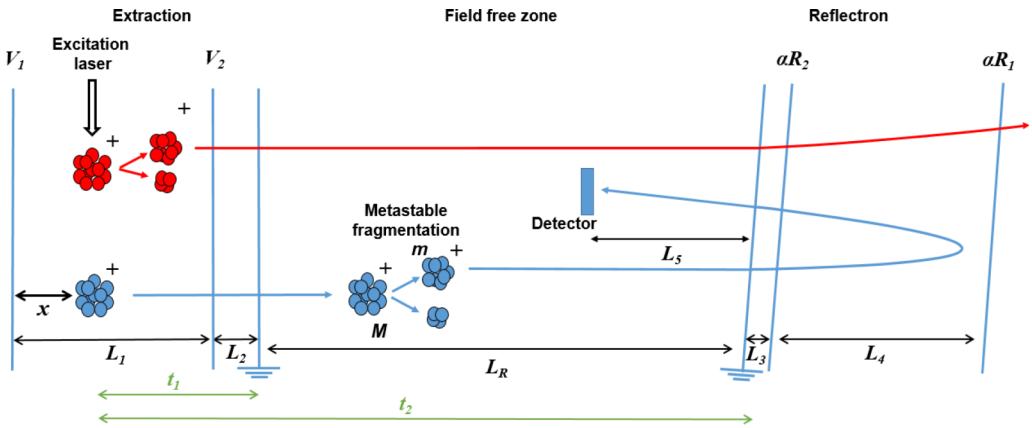

FIG. 1. Schematic overview of the apparatus (not to scale) depicting the regions of laser excitation, ion extraction, free flight, ion reflection, and detection. Important lengths are L_1 = 21 mm, L_2 = 10 mm, L_3 = 10 mm, L_4 = 100 mm, L_5 = 790 mm, and L_R = 1230 mm. The distance x, measured from the first extraction electrode to the point of laser excitation, is x = (12 ± 3) mm. The applied voltages on the extraction and reflectron electrodes are V_1 = 3550 V, V_2 = 2700 V, R_1 = 3593 V, and R_2 = 2336 V at scaling factor α = 1 (discussed in the main text). The times t_1 and t_2, indicated as distances on the figure, are defined in the main text.

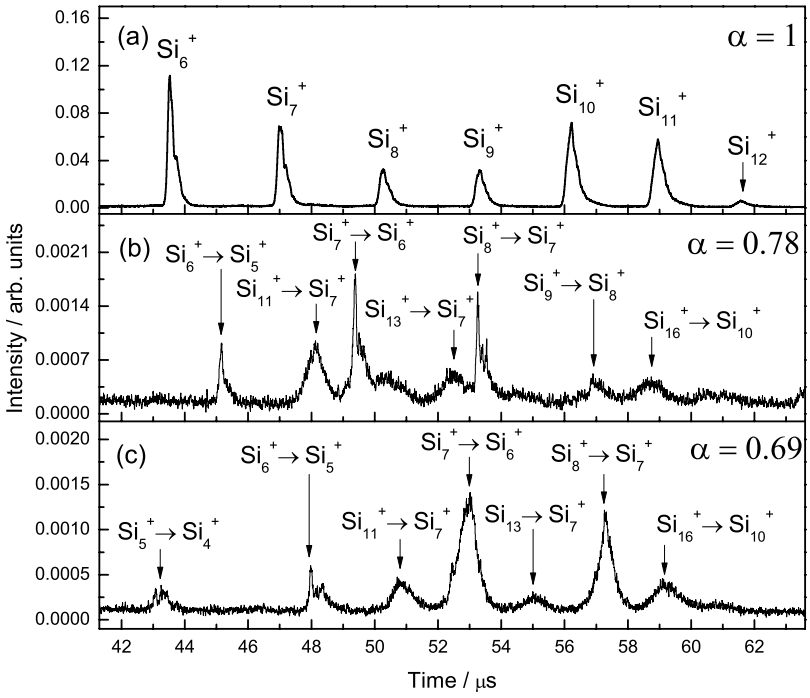

FIG. 2. Time-of-flight spectra for different values of α. In panel (a) ($\alpha = 1$) both the prompt and the metastable fragments are observed, while in panels (b) and (c) ($\alpha < 0.8$) only metastable fragments reach the detector, because the prompt fragments do not turn in the reflectron. The channel dependent effect of changing α becomes clear when comparing the peak corresponding to $Si_6^+ \rightarrow Si_5^+$ with the peak for $Si_{16}^+ \rightarrow Si_{10}^+$. The former shifts by 2.84 μs when the scaling factor is changed from $\alpha = 0.78$ to $\alpha = 0.69$, while the latter shifts only 0.32 μs. The width and asymmetric shape of the peaks in frame (a) are mainly due to the isotopic composition of silicon (92% ^{28}Si, 5% ^{29}Si, and 3% ^{30}Si).

detected at the same flight time. Changing the value of α from unity separated the flight time for clusters that did and those that did not undergo metastable fragmentation during the free flight toward the reflectron. For small values of α, the metastable fragments turn in the reflectron while the more energetic prompt fragments fly through it, ending undetected by the primary detector. Two examples of spectra at reduced reflectron voltages are shown in panels (b) and (c) of Fig. 2.

Tracing the flight time of the metastable peaks with varying α allows to identify the fragmentation pathways, i.e., to assign the masses of both the metastable parent cluster and the fragment. Identification of the parent cluster required measurements over a wide range of reflectron voltages, making use of the fact that a different fragment-to-parent mass ratio implies a different minimal α required to turn the fragments in the reflectron. As a control of the procedure, a detector was placed behind the reflectron to detect the clusters that did not undergo metastable decay. The assignment of the fragmentation pathway is illustrated for two examples in Fig. 3. For a given parent size, different fragment sizes had very different flight times and could easily be distinguished, based on a comparison with calculated flight times for different values of α. See supplementary material for a detailed explanation of the procedure used.[46]

Radiative cooling is measured by delaying ion extraction after laser excitation with a variable delay and tracing the amount of metastable fragmentation as a function of this delay. Reference spectra at $\alpha = 1$ were recorded separately to obtain the parent intensity needed to calculate the metastable fraction, i.e., the ratio of the fragment intensity to the sum of the fragment and parent intensities. The delay between the laser pulse and the switching on of the extraction fields was varied

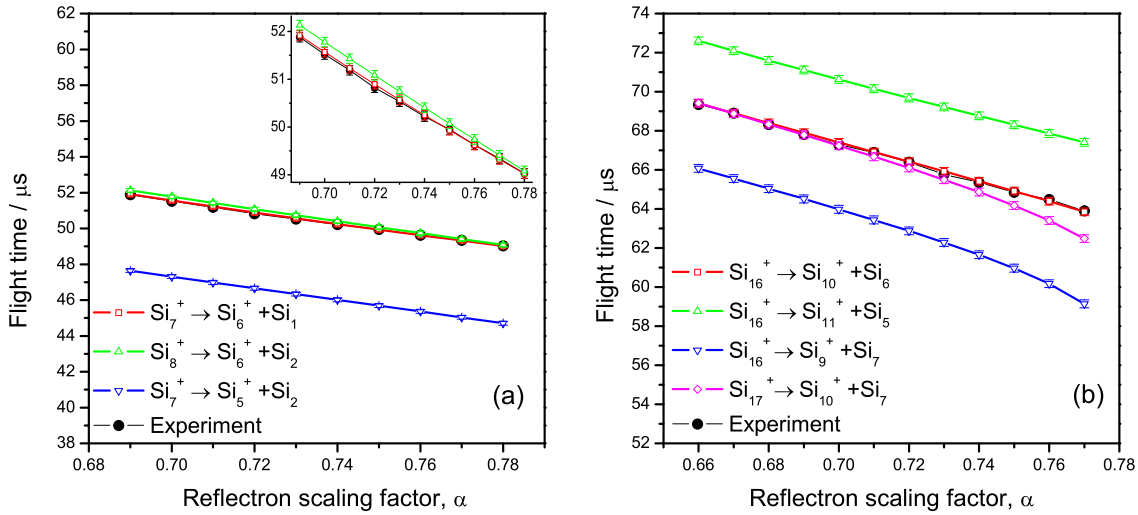

FIG. 3. Examples of assignment of parent and fragment sizes of the metastable fragment peaks. Experimental flight times are compared with calculated values for different fragmentation pathways. The error bars on the modeled points are mainly due to the uncertainty in the position of the excitation laser spot.

between 0 and 1.8 μs. The method has been used previously to study the radiative cooling of laser heated fullerenes[4] and niobium clusters.[3] The two reflectron potentials were reduced to $\alpha = 0.69$ to separate prompt and metastable ionic fragmentation products. The method is based on the fact that in the absence of radiation, the decay will proceed as a power law in time with power -1,[6,47,48] where the time is measured from the laser excitation in the extraction region. The metastable decay between t_1 and t_2 is then proportional to $\ln(t_2/t_1)$, with $t_i = t_{i,0} + \Delta t$ $(i = 1,2)$, where Δt is the delay between the laser pulse and the switching of the extraction voltage, $t_{1,0}$ is the time from the start of the acceleration of the cluster ion to the moment of mass selection in the accelerating stage of the mass spectrometer, and $t_{2,0}$ is the time from the start of the acceleration to the entry into the reflectron. The mass selection in the acceleration occurs when the cluster is somewhere between the starting point and the exit of the acceleration stage. The operational point is set to the time where the clusters have reached half their final kinetic energy. Deviations from this logarithmic decay fraction indicate radiative cooling.

RESULTS AND DISCUSSION

Fragmentation pathways

Table I lists the assigned fragmentation channels. The fragmentation pathways observed in this study are compared with results of earlier photo-excitation[11,18] and collision-induced dissociation[20] experiments on mass selected cationic silicon clusters, also included in the table. The fragmentation pathways could not be reliably determined for $n = 20$ and $n > 21$. For the small clusters with $n < 5$, the metastable decay is suppressed by the small heat capacity of the clusters for well understood reasons (see, e.g., Ref. 49).

The photo-excitation in Ref. 18 produced more charged fragments than the CID experiment, but the dominant products are the same. The multi-collisional CID experiments can be expected to give a more accurate mapping of the lowest energy channels, because the excitation energy is transferred directly into the vibrational motion. The presence of a relatively large number of clusters with more than one decay channel in the CID experiments suggests the presence of sequential decays and/or large energy transfers in those experiments. Therefore, the assignment of the lowest energy channels suffers from some of the same ailments as the photo-excitation experiments in Refs. 11 and 18. In the present experiments, only one fragmentation channel is observed for each cluster size studied. The charged fragment size obtained here is either identical to (for parent sizes Si_n^+, $n = 5$–8, 10–12, 16, 18) or larger (for parent sizes $n = 9$, 13, 15, 17, 19, 21) than the dominant channel in the CID experiments of Ref. 20. For all sizes in the present study, the metastable fragment size observed was a minor channel in Ref. 20, except for Si_{21} where the two experiments even show different channels. Both of these observations strongly suggest that the channels observed here are the lowest energy fragmentation pathways. At this point, a fast sequential decay with an unobserved intermediate species cannot be ruled out without further consideration. This question will be discussed below when the relevant theory has been presented. In addition, the present data resolve the uncertainty of the preferred fragmentation pathways of Si_{13}^+, Si_{17}^+, Si_{19}^+, and Si_{21}^+.

TABLE I. Observed fragmentation products in this study, and the corresponding observed charged decay products after laser excitation (Ref. 11, 532 nm; Ref. 18, 266 nm) and collision induced dissociation.[20] The main charged channels are indicated by bold face. The results in Ref. 18 may include ionization of neutral fragments. The fragments in the last three columns are listed in order of decreasing abundance.

Parent	Charged (neutral) fragment, this work	Charged fragment, Ref. 11	Charged fragment, Ref. 18	Charged fragment, Ref. 20
Si_5^+	**4** (1)	**4**	…	…
Si_6^+	**5** (1)	**5**, 4	…	**5**, 4
Si_7^+	**6** (1)	**6**, 5	…	**6**
Si_8^+	**7** (1)	**7**, 6	…	**7**, 4, 6
Si_9^+	**8** (1)	**6**, 8, 7	…	**6**, 8
Si_{10}^+	**6** (4)	**6**, 7	**6**, 4, 7, 5	**6**
Si_{11}^+	**7** (4)	**7**, 6, 5	**7**, 6, 5, 4, 10	**7**, 6
Si_{12}^+	**6** (6)	**6**, 10, 8[a]	**6**	**6**
Si_{13}^+	**7** (6)	…	**7**, **6**, 12	**6**, 7
Si_{14}^+	**7** (7)	…	**7**, 8, 10, 6	**7**
Si_{15}^+	**10** (5)	…	**8**, 9	**8**, 9
Si_{16}^+	**10** (6)	…	**10**, 6, 4	**10**
Si_{17}^+	**11** (6)	…	**10**, 11, 7	**10**, 11
Si_{18}^+	**11** (7)	…	**11**, 15, 17, 8	**11**
Si_{19}^+	**12** (7)	…	**9**, 10, 6, 7, 12, 13, 16	**9**, 12, 10
Si_{21}^+	**15** (6)	…	**11**, 6, 7, 8, 9, 10	**11**

[a]For these numbers the results from the spectrum shown in Fig. 2 of Ref. 11 are used.

Finally, a comparison with calculated lowest energy channels by DFT simulations should be made. From the many theoretical studies on silicon clusters, Ref. 31, on cationic clusters, was selected for this purpose. The calculated minimum energy structures in Ref. 31 agreed well with the ones assigned by infrared multiple photon dissociation experiments.[36] The studied decay pathways of Si_n^+ (n = 2–13) find that monomer evaporation is the preferred channel for $n \leq 8$ and fragmentation into larger pieces for $n \geq 9$. For all sizes, the calculated preferred fragmentation channel agrees with the current experimental observations, except for $n > 9$, where fragmentation into $Si_5^+ + Si_4$ is computationally predicted while monomer evaporation is the observed channel in this study.

Radiative cooling

The power law decay and the consequent logarithmic dependence of the amount of metastable decay are modified in the presence of thermal radiation. The quenching effect of the radiative cooling on the unimolecular dissociation can be manifested in two different ways. In one, the radiation can be treated as a continuous loss of internal energy, parametrized in terms of an emitted power, without any reference to the wavelength of the emitted photons. This type was observed and quantified in experiments on fullerenes.[4] The size dependent decay rate, R_n, was discussed in Ref. 6 and found to be

$$R_n(t) \propto \frac{1}{e^{w_n t} - 1}, \tag{1}$$

where a non-zero value of w_n indicates the presence of radiation. w_n is related to the radiatively emitted energy by the definition[3]

$$w_n \equiv \frac{d \ln k_n}{dt}, \tag{2}$$

evaluated at the energy where $k_n t = 1$, with k_n the rate constant for unimolecular dissociation. An expression for the right hand side of Eq. (2) will be calculated below.

The other type of radiation pertains to clusters with small heat capacities and/or photons with an energy which is sufficiently large to quench the unimolecular decay completely by emission of a single photon. The modification of the evaporative decay rate for this situation is[50]

$$R_n(t) \propto \frac{e^{-k_{p,n} t}}{t}, \tag{3}$$

where $k_{p,n}$ has a simple interpretation as the photon emission constant for cluster size n. This expression is relevant for electronic transitions with relatively high photon energies and large transition matrix elements compared to, e.g., vibrational transitions. It should be stressed that the description refers to a situation where one or more electronically excited states are thermally populated. In particular, it does not refer to clusters that survive in a specific electronically excited state produced in the initial photo-excitation. Photon emission from thermally excited electronic states has been observed from several different ions, see, e.g., Refs. 5, 51–53, and 50, and there is no reason to exclude this process *a priori* from consideration for silicon clusters.

Note that the nature of the two cooling processes is very different. The use of different symbols (w_n and $k_{p,n}$) emphasizes this fact. Given the very high radiative rate constants reported in this study (see below), one may suspect that Eq. (3) is the relevant equation here, but due to the similar behavior of the two expressions, this cannot be determined by curve fitting. Although the interpretation of the fitted constants is very different in the two cases, the curves are in fact very similar. The main difference between the expressions is that the numerical value assigned to the constants w_n and $k_{p,n}$ differs by 35% from a fit of the same curve. The metastable decay can then be expressed with the same equation in the two cases. Denoting $1/k_{p,n}$ or w_n^{-1} by the common symbol τ_n, the amount of metastable decay[3] is given by

$$M_n = a_n \ln\left(\frac{1 - e^{-(t_{2,0}+\Delta t)/\tau_n}}{1 - e^{-(t_{1,0}+\Delta t)/\tau_n}}\right), \tag{4}$$

where M_n is the metastable fraction, i.e., as defined in the Experimental Procedure section. The parameters a_n, τ_n are positive and cluster specific constants. Fits of the data for τ_n with this expression are the main results for the radiative part of the article. When τ_n is big, the expression reduces to the simpler expression

$$M_n = a_n \left(\ln(t_2/t_1) - \frac{1}{2}(t_2 - t_1)/\tau_n\right). \tag{5}$$

With the delayed extraction protocol used here, the difference $t_2 - t_1$ is constant and as a first estimate τ_n can then be determined from a plot of M_n vs. $\ln(t_2/t_1)$. Such plots provide a fast and robust signature of radiative cooling on the timescale of the experiment (about 20–50 μs). Note that the (unlikely) presence of an amount of cold cationic clusters only affects the fit of the coefficient a_n and not the radiative time constants. Fig. 4 shows two examples of a plot of Eq. (5), one with and one without observable radiative cooling.

To extract a value for τ_n, Eq. (4) is used to fit the metastable decay fraction M_n as a function of delay time Δt. The fitted values are shown in Fig. 5. The values for n = 5, 9, 11, 13 are consistent with the emission of radiation, corresponding to cooling times of 3-13 μs. For the sizes n = 6, 7, 8, no radiation is observed with a 2σ-level criterion. The values of cooling times are on the same order of magnitude as those measured for cationic niobium clusters in the same apparatus,[3] and also of the ones measured for cationic fullerenes.[4,54] This is likely to be related to the high stability and concomitant high internal energy at the evaporation point of all these materials. The cluster temperatures for which these τ_n's are observed are calculated below.

As mentioned, the interpretation of the τ_n's depends on the nature of the emission processes. If, as we suspect, the photons emitted are of an energy so that a single emission quenches the unimolecular decay, the measured (reciprocal) times are simply the Einstein A-coefficients of the excited state times their thermal population.[50]

The alternative continuous cooling requires some analysis before the emitted power can be given. Rewriting Eq. (2), the radiated power P is related to w_n as

$$w_n = \frac{\partial k_n}{\partial T}\frac{dT}{dE}P_n. \tag{6}$$

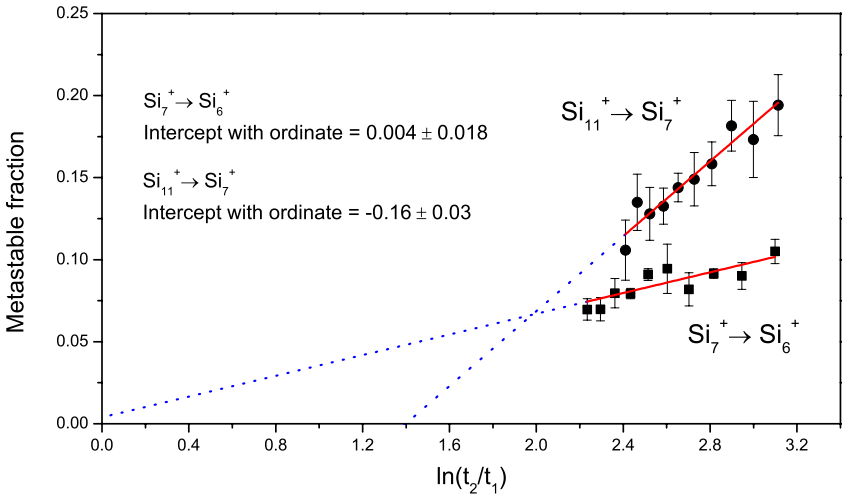

FIG. 4. The metastable decay fraction vs. $\ln(t_2/t_1)$ for Si_7^+ and Si_{11}^+. For the latter, the intercept with the ordinate is clearly below zero, indicating the presence of radiative cooling. For Si_7^+, radiation is not present on the timescale of the experiment.

It is possible to use an Arrhenius expression for the rate constant k_n, if the parameters, including the temperature, are defined properly.[55] Then the relation becomes

$$w_n = \frac{E_{a,n}}{C_n k_B T_e^2} P, \tag{7}$$

where $E_{a,n}$ is the evaporative activation energy, C_n the heat capacity, and T_e the highest temperature in the ion ensemble at time $t = 1/w_n$. The activation energy differs from the true value[55] but is, modulo the extrapolation to finite sizes, the same as the one extracted from a fit to vapor pressure data. Similarly, the heat capacity is an effective value, not equal to the canonical value. The effective temperature, T_e, differs from the microcanonical temperature[56] by the finite heat bath correction (see also Ref. 57).

Although it is not needed for the further analysis, it is instructive to discuss the parts of the parameter space where either Eq. (1) or Eq. (3) is the relevant description of the cooling. This is done by considering the relative change in a rate constant upon photon emission.[58] The crossover photon energy is given by

$$h\nu_0 = E_{a,n} \frac{C_n}{[\ln(\omega t)]^2}. \tag{8}$$

For larger energies, the emission of a single photon will quench the decay and for smaller energies the cooling is best treated as continuous. With values $\ln \omega t = 25$, $E_a = 3$ eV, and $C_v = 3n - 6$, $h\nu_0$ becomes equal to 43 meV for $N = 5$, 260 meV for $N = 20$, and 1.4 eV for $N = 100$. For comparison, black body radiation will have an average photon energy of 480 meV at the temperature of 3 eV/ $\ln \omega t = 1400$ K.

Several results necessary for the application of unimolecular theory for the calculation of w_n are presented in the Appendix, where also G is defined. Combining Eq. (A5) with Eq. (7) gives

$$w_n = \frac{G^2}{C_n E_a} P_n = \frac{P_n}{E_a} \bar{s} e^{G/\bar{s}} (1 - e^{-G/\bar{s}})^2, \tag{9}$$

or

$$P_n = w_n \frac{E_a}{\bar{s}} \frac{e^{-G/\bar{s}}}{(1 - e^{-G/\bar{s}})^2}. \tag{10}$$

For the evaporative activation energy $E_{a,n}$ we use the values from Ref. 25. The emitted power resulting from this analysis is shown in Fig. 6.

We remind the reader that the power shown in Fig. 6 refers to a description of continuous cooling. If instead the cooling proceeds via the emission of a single photon from a thermally populated electronically excited state, the reciprocal

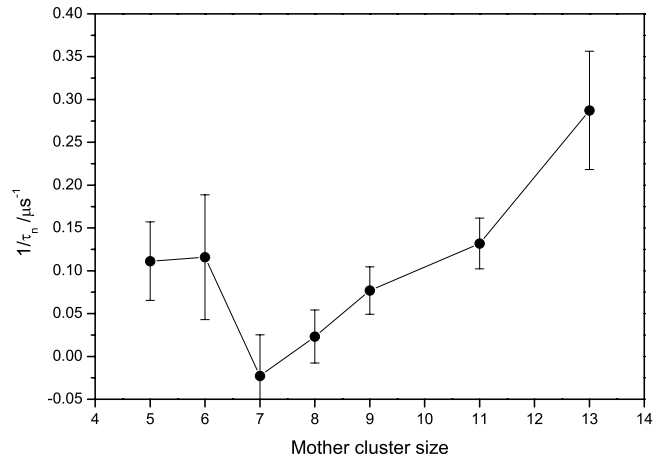

FIG. 5. The radiative cooling rate constant $1/\tau_n$ fitted from the data, with one sigma error bars.

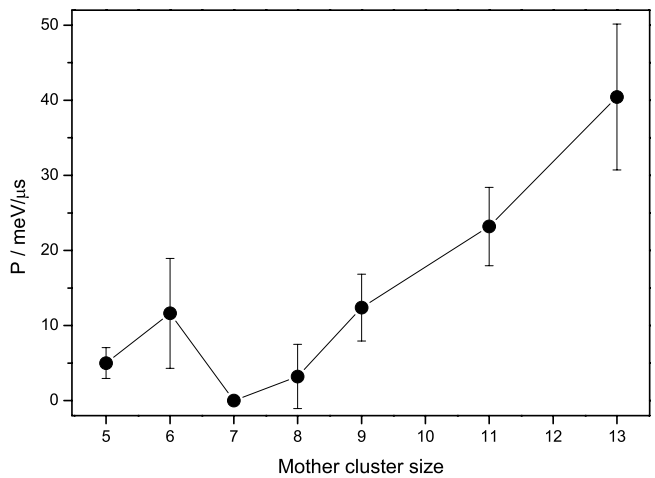

FIG. 6. The emitted power vs. parent cluster size.

time constant, τ_n shown in Fig. 5, is the photon emission rate constant $k_{p,n}$. The high value of A for such states compared with those for vibrational transitions can more than compensate for the smaller thermal population. As mentioned above, such transitions have recently been observed in storage ring experiments on the anthracene anion,[51] C_6^- [52,53] and C_4^-.[50]

The very high power calculated and shown in Figure 6 should be compared with a typical power of the infrared radiation produced by vibrational transitions, which would produce a photon of energy 0.1 eV or less, multiplied by an A-coefficient of 10^2 s^{-1}, or about 10 meV/ms, which is more than a factor 10^3 smaller than the highest power calculated from the data here. Using Eq. (A5) and the activation energies of Ref. 7 ($E_{a,5}$ = 3.8 eV, $E_{a,6}$ = 5.0 eV, $E_{a,7}$ = 4.0 eV, $E_{a,8}$ = 3.9 eV, $E_{a,9}$ = 3.7 eV, $E_{a,10}$ = 3.8 eV, $E_{a,11}$ = 3.9 eV, $E_{a,12}$ = 2.7 eV, $E_{a,13}$ = 2.5 eV), we find the effective emission temperatures to be equal to 2120 K, 2760 K, 2190 K, 2120 K, 2000 K, 2040 K, 2090 K, 1430 K, and 1330 K for n = 5 through 13. These temperatures are the effective fragmentation temperatures. The microcanonical temperature relevant for photon emission is most likely higher, but because the energy of the emitted photons is not known, a precise value cannot be given.

From the present mass spectrometric data alone it is not possible to assign geometric structures. From a comparison of the radiative cooling rates with structures determined by combined ion mobility and theoretical methods in Ref. 29 and by infrared spectroscopy and theoretical methods in Ref. 36, no clear correlation between geometric shapes and radiation rates arises. Matters are complicated by the elevated temperatures in this study, expected to cause strong deviations from ground state structures. An interesting observation is that the radiative time constants in Fig. 5 do not seem to be correlated with the binding energies given in Ref. 7. The latter determines the effective temperatures of the clusters, so this absence of correlation is significant.

Carbon anions provide an interesting comparison because carbon is also a group IV A element. For C_4^- and C_6^-, Eq. (3) applies with photon emission time constants of approximately 10 μs and photon energies of the two excited states of C_4^- at 1.34 and 2.71 eV, and the single excited state of C_6^- at 2.04 eV (other states contribute but with less amplitude).[50,52] The radiative time constant contrasts strongly with the behavior of C_5^- and C_7^- that both cool by emission of infrared photons with time constants on the order of one ms.[58,59] The geometries of these carbon anions are all linear in their electronic ground state, as determined by ion mobility experiments.[60] The different behavior of these carbon cluster anions can therefore not be ascribed to different geometries, but is instead traced to the difference in electronic structure with low lying states for C_4^- and C_6^-, combined with a high electron affinity which, as seen from Eq. (A5), sets the energy scale of the ions.

Cluster stabilities and ionization energies (IEs)

The binding energies determine the excitation energy or equivalently, the effective temperature at which the clusters decay or radiate, as seen from Eq. (A5). For this reason and because binding energies are of interest in their own right, we have analyzed the data with respect to this aspect as well. The analysis also yields improved values for some ionization energies.

The analysis is restricted to situations where the mass loss occurs in a single evaporation. It is therefore necessary first to consider the possibility that an observed mass loss is the result of two or more decays, of which the last is by necessity significantly faster than the first. This is ruled out for $n \leq 9$ because these clusters lose only a single atom during free flight. In general, the problem can only occur if the dissociation energy of the first product is smaller than the precursor dissociation energy by a significant amount, due to the strong cooling of a cluster during the first evaporation. Judging from Fig. 4 of Ref. 7, dissociation energies go up, not down with mass loss in the size range studied here, and the effect is therefore excluded, also for $n > 9$.

It is therefore possible to use the observed decay pathways to order some of the ionization energies of the neutral silicon clusters. The charged fragment will have the lowest IE of the two. The ordering gives the following sets of inequalities:

$$\begin{aligned} &\mathrm{IE(Si_1) > IE(Si_4) > IE(Si_6) > IE(Si_7)} \\ &\quad > \mathrm{IE(Si_{11}), IE(Si_{12}),} \end{aligned} \tag{11}$$

where a ranking between $IE(Si_{11})$ and $IE(Si_{12})$ is not possible, and

$$\mathrm{IE(Si_1) > IE(Si_5) > IE(Si_{10}),} \tag{12}$$

$$\mathrm{IE(Si_1) > IE(Si_8),} \tag{13}$$

and

$$\mathrm{IE(Si_6) > IE(Si_{15}).} \tag{14}$$

The inequalities are generally consistent with earlier ionization energy measurements,[24,37] but we can reduce the upper limits for $Si_{4,5}^+$ in Ref. 24 significantly because the ionization energy of the Si atom has been measured to 8.151 66 ± 0.000 03 eV.[61] For larger silicon clusters only bracketing ionization energy measurements were made in Ref. 24, and it is possible to give better limits on these results. Given that the temperatures of the clusters are fairly high, the observed absence of parallel channels must mean, conservatively, a difference of at least 0.1 eV in ionization energy. A new upper limit is determined for n = 11, and it is confirmed that the ionization energy of Si_{12} is indeed below that of Si_7. Our results are also consistent with the adiabatic ionization energies reported in Ref. 37, with the remark that we can add the inequality $IE(Si_6) > IE(Si_7)$. Combining the present inequalities with the earlier measurements[24,37,61] results in the IE values that are listed in Table II.

In analogy to the inequalities that can be established for the ionization energies, the observed decay channels imply a number of inequalities among the binding energies. All information is contained in the observed decay channels, which can be used for benchmarking theoretical calculations of total binding energies, but several of the inequalities that can be derived are interesting enough to be mentioned here.

The observed channel is the one with the highest rate constant. Barring major differences in the unimolecular frequency factors as well as changes of the average vibrational

TABLE II. The new values of ionization energies of neutral silicon clusters, given in bold face. The other values given are from Refs. 24, 37, and 61 (for the monomer).

n	IE(Si_n) (eV)	n	IE(Si_n) (eV)
1	8.151 66	12	7.17-7.46
2	>8.49	13	7.17-7.46
3	>8.49	14	7.17-7.46
4	**8.0-8.05**	15	7.17-7.46
5	**8.0-8.05**	16	6.80-6.94
6	7.9	17	7.46-7.53
7	**7.8**	18	6.80-6.94
8	7.46-7.87	19	6.80-6.94
9	7.46-7.87	20	7.47-7.53
10	7.9	21	6.80-6.94
11	**7.46-7.7**	22	5.85-5.95

frequencies with cluster size, the observed channel is the one with the lowest activation energy or, equivalently, the biggest binding energy. We will tentatively assume this is the case. For the decay of Si_6^+, for example, the observed decay channel provides the four inequalities

$$\mathrm{BE}(\mathrm{Si}_5^+) + \mathrm{BE}(\mathrm{Si}_1) > \mathrm{BE}(\mathrm{Si}_{6-k}^+) + \mathrm{BE}(\mathrm{Si}_k), \quad k = 2,3,4,5, \tag{15}$$

where $\mathrm{BE}(\mathrm{Si}_n^q)$ is the (total) binding energy of the Si_n^q cluster. The dataset in Table I gives a total of about 200 such inequalities which involve 40 different binding energies, from $n = 1$ to $n = 20$ for neutral and positively charged species.

Some of the inequalities derived involve two unknowns plus the neutral dimer binding energy, $\mathrm{BE}(Si_2)$, which is equal to 3.17 eV.[62] Defining the binding energy of the neutral monomer as zero, we have

$$\mathrm{BE}(\mathrm{Si}_{4+k}^+) > \mathrm{BE}(\mathrm{Si}_3^+) + (k+1)\mathrm{BE}(\mathrm{Si}_2), \quad k = 0,1,2,3,4. \tag{16}$$

Similarly, one gets for the charged cluster monomer dissociation energies, i.e., the difference between the binding energies $D_{n,1}^+ \equiv \mathrm{BE}(\mathrm{Si}_n^+) - \mathrm{BE}(\mathrm{Si}_{n-1}^+)$, the following lower limits:

$$D_{n,1}^+ > \mathrm{BE}(\mathrm{Si}_2) = 3.17 \text{ eV}, \quad n = 4,5,6,7,8. \tag{17}$$

Although these lower limits are not particularly strong (the bulk cohesive energy per atom is 4.6 eV[63]), they are also not completely trivial. From the decay of Si_{10}^+ and Si_{11}^+, one derives for the neutral clusters

$$\mathrm{BE}(\mathrm{Si}_4) > \frac{1}{2}\left(\mathrm{BE}(\mathrm{Si}_3) + \mathrm{BE}(\mathrm{Si}_5)\right), \tag{18}$$

and from the decay of Si_{18}^+ and Si_{19}^+ one has

$$\mathrm{BE}(\mathrm{Si}_7) > \frac{1}{2}\left(\mathrm{BE}(\mathrm{Si}_6) + \mathrm{BE}(\mathrm{Si}_8)\right). \tag{19}$$

Finally, the decay of Si_{12}^+ and Si_{13}^+ gives the inequality

$$\mathrm{BE}(\mathrm{Si}_6) > \frac{1}{2}\left(\mathrm{BE}(\mathrm{Si}_5) + \mathrm{BE}(\mathrm{Si}_7)\right). \tag{20}$$

SUMMARY

The pathways of delayed fragmentation of positively charged silicon clusters after laser excitation have been measured in a reflectron time-of-flight mass spectrometer for clusters composed of 5, 19, and 21 atoms. All clusters decayed via a single pathway, with higher masses of the charged fragments than found previously in both collision induced dissociation and photo-fragmentation experiments. The channels measured here are most likely the lowest activated energy channels. The radiative cooling of seven clusters was measured by the quenching effect on the metastable decay. The shortest radiative cooling time was 3 μs. If the cooling can be considered continuous this corresponds to a radiative power of 40 ± 10 meV/μs, but the values varied strongly with cluster size. Several binding energy inequalities were derived from the data, and previously published brackets on ionization energies could be narrowed. Even though the emitted photons have not been characterized, due to the experimental challenge to measure photons emitted by a dilute and fast moving ion cloud, this work has shown that the emission of radiation is an important cooling mechanism in small silicon clusters.

ACKNOWLEDGMENTS

This work is supported by the Research Foundation - Flanders (FWO) and by the KU Leuven Research Council (BOF program and Grant No. GOA/14/007). P. Ferrari acknowledges CONICyT for BECAS CHILE scholarship.

APPENDIX: THE CLUSTER TEMPERATURE

To apply Eq. (7), first the frequency factor in the Arrhenius expression is determined. For this purpose, the six highest vapor pressure points in Table VII of Ref. 13 are fitted with the function[3]

$$\frac{p}{\sqrt{k_B T}} = \left(\frac{\pi m}{8}\right)^{1/2} \Omega e^{-E_a/k_B T}, \tag{A1}$$

where m is the reduced mass of the monomer and daughter cluster, Ω the Arrhenius frequency factor per unit area, and p the vapor pressure. The fit gives the value $1.8 \cdot 10^{33}$ 1/s $\cdot m^2$ for Ω. With a geometric capture cross section σ of 8.9 Å$^2 n^{2/3}$, calculated from the bulk density, the frequency factor becomes

$$\omega = \Omega\sigma = 1.6 \cdot 10^{14} n^{2/3} \text{ s}^{-1}. \tag{A2}$$

Next, the effective degrees of freedom, $\bar{s}$, are calculated. $\bar{s}$ is the average canonical heat capacity of reactant and products, in units of k_B. The heat capacity of bulk silicon is temperature dependent, and we use the value, corresponding to the experimentally measured bulk value at 2000 K, of

$$\bar{s} = 1.1(3\bar{n} - 6) = 1.1(3n - 7.5), \tag{A3}$$

where $\bar{n}$ is the average number of atoms in the reactant and product clusters. This corresponds to the loss of a neutral atom, which is the observed channel for $n \leq 9$. For larger cluster sizes, the value is slightly different because the neutral fragment is then a molecule which reduces vibrational and

increases rotational degrees of freedom of the product state, giving $\bar{s} = 1.1(3n-9)+1.5$ from $n = 10$ and upwards. For simplicity, we will use the expression in Eq. (A3) for all sizes. Defining the parameter $G \equiv \ln(\omega/\tau_n)$ or $G \equiv \ln(\omega t_{0,1})$, whichever is the smallest, we can write the effective heat capacity as[55]

$$C_n = \frac{G^2}{\bar{s}} e^{-G/\bar{s}} \left(1 - e^{-G/\bar{s}}\right)^{-2}. \tag{A4}$$

Without any appreciable loss of accuracy we can use the values $G = 18.9 + \frac{7}{6}\ln(n)$, corresponding to a timescale proportional to $n^{1/2}$ and an Arrhenius frequency factor proportional to $n^{2/3}$.

This value is also used in the calculation of the effective temperature, viz., $\mathrm{w}_n = \omega \exp(-E_a/k_B T_e)$ (replacing w by $1/t_{0,1}$ if the former is zero). This gives

$$T_e = E_{a,n}/\ln(\omega/\mathrm{w}_n) = \frac{E_{a,n}}{G}. \tag{A5}$$

[1]U. Frenzel, U. Hammer, H. Westje, and D. Kreisle, Z. Phys. D: At., Mol. Clusters **40**, 108–110 (1997).
[2]C. Walther, G. Dietrich, W. Dostal, K. Hansen, S. Kruckeberg, K. Lutzenkirchen, and L. Schweikhard, Phys. Rev. Lett. **83**, 3816 (1999).
[3]K. Hansen, Y. Li, V. Kaydashev, and E. Janssens, J. Chem. Phys. **141**, 024302 (2014).
[4]K. Hansen and E. E. B. Campbell, J. Chem. Phys. **104**, 5012 (1996).
[5]J. U. Andersen, C. Brink, P. Hvelplund, M. O. Larsson, B. B. Nielsen, and H. Shen, Phys. Rev. Lett. **77**, 3991 (1996).
[6]K. Hansen, J. U. Andersen, P. Hvelplund, S. P. Møller, U. V. Pedersen, and V. V. Petrunin, Phys. Rev. Lett. **87**, 123401 (2001).
[7]M. F. Jarrold and E. C. Honea, J. Phys. Chem. **95**, 9181 (1991).
[8]C. E. Richter and M. Trapp, Int. J. Mass Spectrom. Ion Phys. **38**, 21 (1981).
[9]T. T. Tsong, Appl. Phys. Lett. **45**, 1149 (1984).
[10]J. R. Heath, Y. Liu, S. C. O'Brien, Q. L. Zhang, R. F. Curl, F. K. Tittel, and R. E. Smalley, J. Chem. Phys. **83**, 5520 (1985).
[11]L. A. Bloomfield, R. R. Freeman, and W. L. Brown, Phys. Rev. Lett. **54**, 2246 (1985).
[12]T. P. Martin and H. Schaber, J. Chem. Phys. **83**, 855 (1985).
[13]P. D. Desai, J. Phys. Chem. Ref. Data **15**, 967 (1986).
[14]Y. Liu, Q. L. Zhang, F. K. Tittel, R. F. Curl, and R. E. Smalley, J. Chem. Phys. **85**, 7434 (1986).
[15]D. Tománek and M. A. Schlüter, Phys. Rev. Lett. **56**, 1055 (1986).
[16]D. J. Trevor, D. M. Cox, K. C. Reichmann, R. O. Brickman, and A. Kaldor, J. Phys. Chem. **91**, 2598 (1987).
[17]O. Cheshnovsky, S. H. Yang, C. L. Pettiette, M. J. Craycraft, Y. Liu, and R. E. Smalley, Chem. Phys. Lett. **138**, 119 (1987).
[18]Q. Zhang, Y. Liu, R. F. Curl, F. K. Tittel, and R. E. Smalley, J. Chem. Phys. **88**, 1670 (1988).
[19]K. Raghavachari and C. M. Rohlfing, J. Chem. Phys. **89**, 2219 (1988).
[20]M. F. Jarrold and J. E. Bower, J. Phys. Chem. **92**, 5702 (1988).
[21]S. M. Beck and J. M. Andrews, J. Chem. Phys. **91**, 4420 (1989).
[22]W. Begemann, R. Hector, Y. Y. Liu, J. Tiggesbäumker, K. H. Meiwes-Broer, and H. O. Lutz, Z. Phys. D: At., Mol. Clusters **12**, 229 (1989).
[23]E. C. Honea, A. Ogura, C. Murray, K. Raghavachari, W. O. Sprenger, M. F. Jarrold, and W. L. Brown, Nature **366**, 42 (1993).
[24]K. Fuke, K. Tsukamoto, F. Misaizu, and M. Sanekata, J. Chem. Phys. **99**, 7807 (1993).
[25]A. A. Shvartsburg, M. F. Jarrold, B. Liu, Z.-Y. Lu, C.-Z. Wang, and K.-M. Ho, Phys. Rev. Lett. **81**, 4616 (1998).
[26]K.-M. Ho, A. A. Shvartsburg, B. Pan, Z.-Y. Lu, C.-Z. Wang, J. G. Wacker, J. L. Fye, and M. F. Jarrold, Nature **392**, 582 (1998).
[27]C. Xu, T. R. Taylor, G. R. Burton, and D. M. Neumark, J. Chem. Phys. **108**, 1395 (1998).
[28]B. Liu, Z.-Y. Lu, B. Pan, C.-Z. Wang, K.-M. Ho, A. A. Shvartsburg, and M. F. Jarrold, J. Chem. Phys. **109**, 9401 (1998).
[29]A. A. Shvartsburg, R. R. Hudgins, P. Dugourd, and M. F. Jarrold, Chem. Soc. Rev. **30**, 26 (2001).
[30]X. Zhu and X. C. Zeng, J. Chem. Phys. **118**, 3558 (2003).
[31]S. Nigam, C. Majumder, and S. K. Kulshreshtha, J. Chem. Phys. **121**, 7756 (2004).
[32]C. Pouchan, D. Bégué, and D. Y. Zhang, J. Chem. Phys. **121**, 4628 (2004).
[33]J. Yang, W. Xu, and X. Wensheng, J. Mol. Struct.: THEOCHEM **719**, 89 (2005).
[34]M. A. Belkhir, S. Mahtout, M. Belabbas, and I. Samah, Physica E **31**, 86 (2006).
[35]W. Qin, W.-C. Lu, L.-Z. Zhao, Q.-J. Zang, C. Z. Wang, and K. M. Ho, J. Phys.: Condens. Matter **21**, 455501 (2009).
[36]J. Lyon, P. Gruene, A. Fielicke, G. Meijer, E. Janssens, P. Claes, and P. Lievens, J. Am. Chem. Soc. **131**, 1115 (2009).
[37]O. Kostko, S. R. Leone, M. A. Duncan, and M. Ahmed, J. Phys. Chem. A **114**, 3176 (2010).
[38]M. Haertelt, J. T. Lyon, P. Claes, J. de Haeck, P. Lievens, and A. Fielicke, J. Chem. Phys. **136**, 064301 (2012).
[39]M. Vogel, C. Kasigkeit, K. Hirsch, A. Langeberg, J. Rittmann, V. Zamudio-Bayer, A. Kulesza, R. Mitric, T. Moller, B. v. Issendorff, and J. T. Lau, Phys. Rev. B **85**, 195454 (2012).
[40]P. Claes, E. Janssens, V. T. Ngan, P. Gruene, J. T. Lyon, D. J. Harding, A. Fielicke, M. T. Nguyen, and P. Lievens, Phys. Rev. Lett. **107**, 173401 (2011).
[41]P. Claes, V. T. Ngan, M. Haertelt, J. T. Lyon, A. Fielicke, M. T. Nguyen, P. Lievens, and E. Janssens, J. Chem. Phys. **138**, 194301 (2013).
[42]Y. Li, J. T. Lyon, A. P. Woodham, P. Lievens, A. Fielicke, and E. Janssens, J. Phys. Chem. C **119**, 10896 (2015).
[43]P. Gruene, A. Fielicke, G. Meijer, E. Janssens, V. T. Ngan, M. T. Nguyen, and P. Lievens, ChemPhysChem **9**, 703 (2008).
[44]V. T. Ngan, P. Gruene, P. Claes, E. Janssens, A. Fielicke, M. T. Nguyen, and P. Lievens, J. Am. Chem. Soc. **132**, 15589 (2010).
[45]W. Bouwen, P. Thoen, F. Vanhoutte, S. Bouckaert, F. Despa, H. Weidele, R. E. Silverans, and P. Lievens, Rev. Sci. Instrum. **71**, 54 (2000).
[46]See supplementary material at http://dx.doi.org/10.1063/1.4936917 for details of the fragment size assignment.
[47]J. U. Andersen, H. Cederquist, J. S. Forster, B. A. Huber, P. Hvelplund, J. Jensen, B. Liu, B. Manil, L. Maunoury, S. Brøndsted Nielsen, U. V. Pedersen, H. T. Schmidt, S. Tomita, and H. Zettergren, Eur. Phys. J. D. **25**, 139 (2003).
[48]J. U. Andersen, E. Bonderup, K. Hansen, P. Hvelplund, B. Liu, U. V. Pedersen, and S. Tomita, Eur. Phys. J. D **24**, 191 (2003).
[49]K. Hansen and U. Näher, Phys. Rev. A **60**, 1240 (1999).
[50]N. Kono, T. Furukawa, H. Tanuma, J. Matsumoto, H. Shiromaru, T. Azuma, K. Najafian, M. S. Pettersson, B. Dynefors, and K. Hansen, Phys. Chem. Chem. Phys. **17**, 24732 (2015).
[51]S. Martin, J. Bernard, R. Brédy, B. Concina, C. Joblin, M. Ji, C. Ortega, and L. Chen, Phys. Rev. Lett. **110**, 063003 (2013).
[52]G. Ito, T. Furukawa, H. Tanuma, J. Matsumoto, H. Shiromaru, T. Majima, M. Goto, T. Azuma, and K. Hansen, Phys. Rev. Lett. **112**, 183001 (2014).
[53]V. Chandrasekaran, B. Kafle, A. Prabhakaran, O. Heber, M. Rappaport, H. Rubinstein, D. Schwalm, Y. Toker, and D. Zajfman, J. Phys. Chem. Lett. **5**, 4078 (2014).
[54]S. Tomita, J. U. Andersen, C. Gottrup, P. Hvelplund, and U. V. Pedersen, Phys. Rev. Lett. **87**, 073401 (2001).
[55]K. Hansen, Chem. Phys. Lett. **620**, 43 (2015).
[56]J. U. Andersen, E. Bonderup, and K. Hansen, J. Chem. Phys. **114**, 6518 (2001).
[57]C. E. Klots, J. Chem. Phys. **90**, 4470 (1989).
[58]K. Najafian, M. S. Pettersson, B. Dynefors, H. Shiromaru, J. Matsumoto, H. Tanuma, T. Furukawa, T. Azuma, and K. Hansen, J. Chem. Phys. **140**, 104311 (2014).
[59]M. Goto, A. E. K. Sundén, H. Shiromaru, J. Matsumoto, H. Tanuma, T. Azuma, and K. Hansen, J. Chem. Phys. **139**, 054306 (2013).
[60]G. von Helden, P. R. Kemper, N. G. Gotts, and M. T. Bowers, Science **259**, 1300 (1993).
[61]C. M. Brown, S. G. Tilford, R. Tousey, and M. L. Ginter, J. Opt. Soc. Am. **64**, 1665 (1974).
[62]M. W. Chase, C. A. Davies, J. R. Downey, Jr., D. J. Frurip, R. A. McDonald, and A. N. Syverud, J. Phys. Chem. Ref. Data **14**, 1 (1985).
[63]B. Farid and R. W. Godby, Phys. Rev. B **43**, 14248 (1990).